RESEARCH ARTICLE
SPACE PHYSICS: IONOSPHERIC PHYSICS

Earth and Planetary Physics
9: 387–399, 2025
doi: 10.26464/epp2025012

Modulated waveforms for harmonic minimization of far-field signals in amplitude-modulated heating of the ionosphere

ZhiJian Lu[1], Yong Li[1,2], Hui Li[2], Jian Wu[1,2], JingFeng Yao[1,3,4], XingBao Lyu[1,3,4], ChengXun Yuan[1,3,4], ZhongXiang Zhou[1,3,4]*, and Ying Wang[1,3,4]

[1]School of Physics, Harbin Institute of Technology, Harbin 150001, China;

[2]China Research Institute of Radio Waves Propagation, Beijing 102206, China;

[3]Heilongjiang Provincial Key Laboratory of Plasma Physics and Application Technology, Harbin 150001, China;

[4]Heilongjiang Provincial Innovation Research Center for Plasma Physics and Application Technology (International Cooperation), Harbin 150001, China

Key Points:

- A modulation amplitude heating model is established, and the specific height of the radiation source region is determined.
- A new modulation waveform is proposed, which significantly reduces the proportion of harmonic energy in the far-field signals generated by amplitude modulation heating.
- It is confirmed that the ability of the modulation waveform to suppress harmonics is unaffected by changes in modulation frequency and effective radiated power.

Citation: Lu, Z. J., Li, Y., Li, H., Wu, J., Yao, J. F., Lyu, X. B., Yuan, C. X., Zhou, Z. X., and Wang, Y. (2025). Modulated waveforms for harmonic minimization of far-field signals in amplitude-modulated heating of the ionosphere. *Earth Planet. Phys.*, *9*(2), 387–399. http://doi.org/10.26464/epp2025012

Abstract: This paper establishes an amplitude modulation heating model, simulating the far-field radiation of ELF/VLF signals generated by modulation heating, as well as the specific location and longitudinal extent of the radiation source. We consider various modulation waveforms and find that square-wave modulation has the highest excitation efficiency for ELF/VLF signals, and that square-wave modulation with a smaller duty cycle (<50%) exhibits higher excitation efficiency for ELF/VLF signals, while the $\sin^2 t$ waveform modulation yields the lowest proportion of harmonic energy in the generated signals. The amplitude of the second harmonic generated by the $\sin^2 t$ waveform is less than one-tenth that of the fundamental frequency, and the energy of higher-frequency harmonics can be negligibly small compared with those of the fundamental wave. It is a challenging task to achieve a balance between enhancing the excitation efficiency of ELF/VLF signals and also suppressing harmonics generated by the modulated heating process. This is because the harmonics are correspondingly enhanced as the excitation efficiency of the signals is increased. However, we find that under conditions of varying effective radiant power and modulation frequency, as long as the modulation waveform is unchanged, the energy ratio between the fundamental frequency signal generated by modulated heating and each harmonic is relatively fixed, with changes only in signal intensity and the location of the radiation source zone. This implies that one can first select modulation waveforms that make the signal less prone to distortion, then increase the effective radiated power to enhance the signal strength, without concern for harmonic interference of the fundamental signal.

Keywords: ELF/VLF; harmonic; amplitude-modulated heating; modulated waveforms

1. Introduction

Tellegen's discovery of the "Luxembourg effect" (Tellegen, 1933) prompted expanded exploration into ways of artificially modifying the ionosphere. Modulated heating of the ionosphere can generate "virtual antennas" in the D-region that emit extremely low frequency (ELF) and very low frequency (VLF) waves to the external environment. These electromagnetic waves have significant applications in fields such as subsurface material exploration and covert communication (Li JF et al., 2023a, b).

After several facilities were constructed to study ionosphere heating, the theories and models regarding the interaction between electromagnetic waves and the ionosphere proposed by Bailey and Martyn (1934), Farley (1963), Willis and Davis (1973), and others have been experimentally verified. Experimental studies into modulated heating of the ionosphere have also been conducted, shifting the focus from theory to practical experiments. Many notable experimental phenomena have been observed, such as significant increases in the electron temperature of the ionosphere and the development of the F-region through heating by a high-frequency transmitting facility (Utlaut, 1970;

First author: Z. J. Lu, 21s011050@stu.hit.edu.cn
Correspondence to: Z. X. Zhou, zhouzx@hit.edu.cn
Received 31 MAY 2024; Accepted 22 NOV 2024.
First Published online 09 JAN 2025.

Utlaut and Violette, 1974). The amplitude modulation heating ionospheric experiment conducted at the Arecibo observatory enabled the ground receiving station to successfully detect near-field ELF/VLF signals with an intensity of approximately 1 fT, thereby confirming the theoretical concept of constructing ELF/VLF antennas through artificial modulation of the ionospheric currents. (Getmantsev et al., 1974; Ferraro et al., 1982).

To make use of the ELF/VLF signals generated by modulated heating in communication systems, it is necessary to enhance the strength of the signal and minimize its distortion. Experimental research on increasing signal excitation intensity has revealed the relationship between excitation signal strength and heating power, polarization direction (Ferraro et al., 1984), and natural electric field magnitude (Yang JT et al., 2019). In addition, rapid scanning techniques (Papadopoulos et al., 1990), pre-heating methods (Milikh and Papadopoulos, 2007), and geometric modulation heating methods (Cohen et al., 2010) have been proposed, and have successfully increased the signal strength by several tens of decibels. Further experiments compared the intensity of electromagnetic signals emitted from the ionosphere at different latitudes under the same heating conditions. The results indicated that the intensity of ELF/VLF signals generated by modulation heating at low or middle latitudes is several orders of magnitude weaker than that at high latitudes (Ferraro et al., 1984; Moore et al., 2007; Cohen et al., 2008). This is attributed to the significantly weaker natural electric fields in the ionosphere at low or middle latitudes compared to high latitudes. Consequently, amplitude modulation heating schemes are typically applied only in high latitude regions.

When the ionosphere is heated, collisions between electrons and other particles become more intense, leading to an increasing loss of electron energy. The growth rate of the electron temperature gradually slows down instead of remaining constant, until the electron temperature reaches a new steady state, at which point the electron temperature growth rate drops to 0. As a result, the high-frequency wave heating of the ionosphere becomes a nonlinear process in which the trend of electron temperature change does not necessarily align with the variation in heating power. Therefore, in modulated heating experiments, besides exciting the fundamental frequency signal, a series of harmonics are also generated. These harmonics can cause issues such as signal distortion and spectrum broadening.

Research on suppressing the proportion of harmonics in the signal revolves mainly around modulated waveforms. For instance, Rowland et al. (1996) analyzed the energy proportions of various harmonics in a square-wave modulated heating experiment signal of the High-Power Auroral Stimulation (HIPAS) facility. Kuo SP et al. (1998) compared simulations using square-wave and beat-wave modulation waveforms, determining that beat-wave modulation produces higher signal quality. Jin G et al. (2012) proposed the inv-sin waveform achieved through numerical inversion, significantly reducing harmonic intensity.

Due to the long wavelengths of ELF/VLF signals and limited heating power, the generated ELF/VLF signals are weak and unstable (Cohen et al., 2008; Cohen and Gołkowski, 2013), with low conversion efficiency (defined as the energy ratio between the heating wave and the generated electromagnetic signal). Moreover, receiving stations are often located relatively close to the heating stations. Current discussions on minimizing harmonics in modulated heating focus primarily on near-field signal areas. With the development of heating devices, the effective radiant power output has been significantly increased, and the ELF/VLF signals excited in the ionosphere have become stronger (Cohen and Gołkowski, 2013; Streltsov et al., 2018), so that the signals can be detected at greater distances (Moore et al., 2007), opening up the possibility of future long-distance communications such as satellite newsletter (Lu H et al., 2021). Reducing the harmonic content in far-field signals and maximizing the excitation efficiency of ELF/VLF signals are therefore important considerations.

In this study, we establish an amplitude modulation heating model that make it possible to calculate disturbances in ionospheric conductivity during modulation. This model determines the specific location and scale of the radiation source zone, as well as the energy relationship between the fundamental frequency and harmonics of the excited ELF/VLF signal. This allows us to compare changes in output signals by altering heating conditions (modulation waveform, effective radiated power, modulation frequency) and provide explanations for these changes. Ultimately, we aim to obtain the modulation waveform with the highest excitation efficiency and the minimum harmonics.

2. Theoretical Model

2.1 Ohmic Heating Model

High-power HF electromagnetic waves are used to heat the ionosphere. In regions with high neutral particle density, such as the D and E layers, electrons are accelerated by the electric field of the incident wave. Subsequently, through frequent collisions with other particles (ions and neutral particles), the energy of electrons is transferred to those particles. After a certain period, the energy absorbed by electrons from the heating wave equals the energy of electrons lost through collisions. Then, electron temperature stabilizes. This physical mechanism can be explained using ohmic heating theory.

Amplitude modulation heating involves setting a modulation frequency within the desired frequency range of the heating wave. This modulation frequency causes the amplitude of the heating wave to vary during the heating process. The heated region of the ionospheric experiences "heating" and "cooling" states within one modulation cycle. Variables such as electron temperature and conductivity in the ionosphere undergo periodic disturbances at the modulation frequency, leading to oscillating currents that radiate signals of corresponding frequencies to the external environment.

During ionosphere heating, electrons both gain and lose energy through collisions with particles and other processes. The electron energy equation (Rietveld et al., 1986; Li Y et al., 2023c) can be written:

$$\frac{3}{2}k_{\mathrm{b}}N_{\mathrm{e}}\frac{\partial T_{\mathrm{e}}}{\partial t}=Q\left(T_{\mathrm{e}},h\right)-L\left(T_{\mathrm{e}},h\right), \tag{1}$$

where k_b is the Boltzmann constant, T_e is electron temperature. h is altitude above the ground, Q is the energy gained by electrons per unit time and per unit volume, L is electron energy loss per unit time and per unit volume (Stubbe and Varnum, 1972), and N_e is electron density. An expression for the absorption term Q for the heating wave energy per unit time and per unit volume at altitude h is:

$$Q(T_e, h) = 2\frac{\omega}{c}\chi S(h), \tag{2}$$

where χ is the absorption rate of energy (Li H and Wu J, 2021), and S is the energy density of electromagnetic waves, a function of altitude. This can be expressed as:

$$S(h) = \frac{P_E}{4\pi h^2}\exp\left(-2\int_{h_0}^{h}\chi(h')\,\mathrm{d}h'\right), \tag{3}$$

where P_E is the effective radiated power of the heating wave, and h_0 is the lower boundary of the ionosphere. In Equation (1), L is the loss term of electron energy, it results from elastic collisions between electrons and various particles as well as inelastic collisions and the excitation of various particle rotation states, vibration states, electron states, and fine structures. When the left side of the Equation (1) equals 0, indicating equilibrium, the electron temperature at the corresponding altitude can be obtained.

The variation of electron density during the heating process can be described by the electron continuity equation:

$$\frac{\partial n_e}{\partial t} = q - \alpha(T_e)\,n_e^2, \tag{4}$$

where q is the electron production rate, n_e is electron density and $\alpha(T_e)$ is a recombination coefficient obtained from empirical formulas (Gurevich, 1976):

$$\alpha(T_e) = 5\times10^{-7}\left[NO^+\right](300/T_e)^{1.2} + 2.2\times10^{-7}\left[O_2^+\right](300/T_e)^{0.7}, \tag{5}$$

where $[NO^+]$ and $[O_2^+]$ are the NO^+ and O_2^+ molecular ion concentrations. This formula ignores complex chemical processes such as electron loss caused by negative ions and hydrated ions; it considers only the dissociation and complex reactions of NO^+ and O_2^+:

$$NO^+ + e \rightarrow N + O, \tag{6}$$

$$O_2^+ + e \rightarrow O + O. \tag{7}$$

2.2 Amplitude-modulated Heating Model

The heating wave injected into the ionosphere increases the electron temperature and changes the electron collision frequency and ion collision frequency, thus affecting the magnitude of conductivity. This leads to oscillating currents, forming an equivalent dipole moment in the ionosphere, which radiates ELF/VLF band waves to the external environment. The magnitude of the oscillating current generated by modulation heating is described by:

$$\Delta\boldsymbol{J} = E_0\Delta\sigma, \tag{8}$$

where E_0 is the natural electric field. $\Delta\sigma = \hat{x}\Delta\sigma_H + \hat{y}\Delta\sigma_P$ represents the perturbation of the conductivity in the ionosphere, where $\Delta\sigma_H$ and $\Delta\sigma_P$ denote the Hall conductivity and Pedersen conductivity, respectively. (Zhou KJ et al., 2020):

$$\Delta\sigma_H = -2\frac{N_e e}{B}\frac{\nu_e\omega_{ce}^2}{\nu_e^2+\omega_{ce}^2}\frac{\mathrm{d}\nu_e}{\mathrm{d}T_e}\Delta T_e, \tag{9}$$

$$\Delta\sigma_P = \frac{N_e e}{B}\frac{\omega_{ce}\left(\omega_{ce}^2-\nu_e^2\right)}{\nu_e^2+\omega_{ce}^2}\frac{\mathrm{d}\nu_e}{\mathrm{d}T_e}\Delta T_e, \tag{10}$$

where e is the unit electron charge, ω_{ce} is the electron cyclotron frequency, and ν_e is the electron collision frequency, which can be expressed by the following equation (Pashin et al., 1995):

$$\nu_e = 1.7\times10^{-11}[N_2]T_e + 3.8\times10^{-10}[O_2]T_e^{0.5} + 1.4\times10^{-10}[O]T_e^{0.5}. \tag{11}$$

The strength of the radiation signal received by the ground receiving station can be expressed as (Kuo SP, 2018):

$$\boldsymbol{B} = -\frac{\mu_0 V}{4\pi}\left(\frac{\boldsymbol{J}}{r^2} + \frac{1}{rv_A}\frac{\partial\boldsymbol{J}}{\partial t}\right), \tag{12}$$

where V is the volume disturbance caused by heating; the first term within the parentheses represents near-field radiation, and the second term represents far-field radiation; μ_0 is the permeability of free space; r is the distance between the receiving point and the radiation source; $\boldsymbol{J}$ is the current density in the ionosphere; and v_A is the average phase velocity of the propagating radiation signal from the ionosphere to the receiving station.

From Equation (12), it can be inferred that the strength of the far-field signal depends mainly on the magnitude of the first-order time derivative of the oscillating current. The oscillating current can be calculated from the change in conductivity with time during the modulated heating of the ionosphere, and observing the changes of $\partial\sigma/\partial t$ in the ionosphere during modulation heating allows for an understanding of the quality of the ELF/VLF signals.

3. Simulation Results and Discussion

We chose the EISCAT facility (69.6°N, 19.2°E) in high-latitude regions for the simulation, with ionospheric data from the altitude range of 65 km to 120 km taken at 12:00 UT on December 4, 2018. Data for electron temperature, electron density, and concentration of ions (NO^+, O_2^+) in the ionosphere are from the IRI 2020 (International Reference Ionosphere 2020) model, and data for the concentration of neutral particles (N_2, O_2, O) are from the NRLMSIS 2.0 (Naval Research Laboratory mass spectrometer and incoherent scatter radar 2.0) model. The effective radiated power was set to 16 MW, with a modulation frequency of 2000 Hz. The heating wave was in the X-band, with a heating wave frequency of 4 MHz. Initially, we applied a square-wave with a duty cycle of 50%, a triangular wave, and a sine wave for modulated heating of the ionosphere. To ensure that the energy within a single modulation cycle is equal for the different waveforms, necessary adjustments were made to the effective radiated power.

3.1 Conductivity Oscillations under Fundamental Waveform Modulation

The time rate of change of Hall conductivity and Pedersen conductivity for different frequency bands at different altitudes in the ionosphere, under modulation heating by a square-wave with a 50% duty cycle, is shown in Figure 1. According to the results, under conditions of supplying the same energy within a single cycle, the positions of the radiation source regions generated by

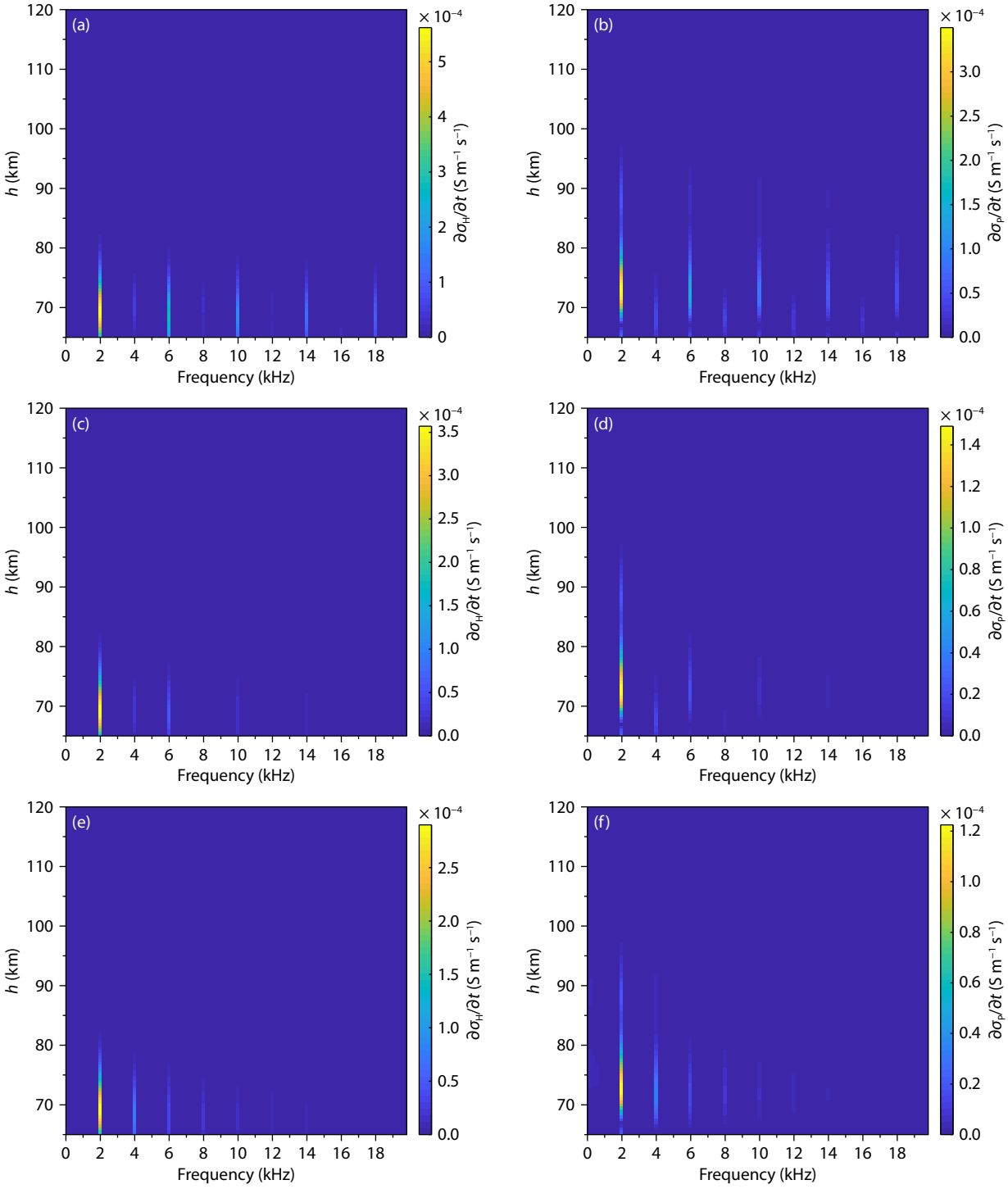

Figure 1. Modulation of the amplitude of the oscillations of the conductivity at each frequency in each height region of the ionosphere during the heating period. (a), (c), and (e): Results of oscillations induced by a square-wave with 50% duty cycle, a triangular wave, and a sine-wave modulation for Hall conductivity, respectively. (b), (d), and (f): Results of oscillations induced by a square-wave with 50% duty cycle, a triangular wave, and a sine wave modulation for Pedersen conductivity, respectively.

the three waveform modulations are generally consistent, concentrated near the D region at an altitude of 70 km. In this context, the maximum values of the fundamental frequency component $\partial\sigma_H/\partial t$ are found in the vicinity of this 70 km altitude, while the maximum values of the component $\partial\sigma_P/\partial t$ are located at 73 km altitude. Within the main radiation source region, the amplitude of $\partial\sigma_H/\partial t$ is much greater than that of $\partial\sigma_P/\partial t$, and the longitudinal size of the Pedersen conductivity disturbance area is much larger than that of the Hall conductivity disturbance area.

In addition, the results indicate that in the signals generated by square-wave with a 50% duty cycle and triangular-wave modulation, the intensity of odd harmonics is significantly greater than that of even harmonics, and the radiation source region for odd

harmonics is larger in volume. In contrast, the sine-wave modulation does not exhibit this characteristic. As the frequency increases, the intensity of harmonics decreases. It can be observed that, generally, triangular-wave modulation has the strongest suppression capability, followed by sine-wave modulation. Additionally, with increasing frequency, the longitudinal size of the radiation source for harmonics generated by sine-wave modulation significantly decreases. On the other hand, square-wave modulation exhibits the greatest distortion in the generated signal, with the excitation of ELF/VLF signals being the strongest.

Comparative analysis of the derivatives of Hall conductivity at 70 km and Pedersen conductivity at 73 km for three waveform modulations at various frequencies is presented in Figure 2. The results indicate that the oscillation amplitudes induced by a square-wave with 50% duty cycle modulation are greater than those for the other two modulation waveforms at the fundamental frequency and odd harmonics. In other words, the radiation signal intensity produced by square-wave modulation is the greatest, but its ability to suppress harmonics is the weakest. In comparison, although the fundamental frequency signal intensity produced by triangular-wave modulation is weaker than that of square-wave modulation, the proportion of harmonic energy in its signal is much smaller. Under the same heating conditions, the fundamental frequency signal produced by the sine-wave is the weakest, with a harmonic suppression capability superior to square-wave modulation, but weaker than triangular wave modulation.

In square-wave modulation, there are moments when energy is suddenly supplied and suddenly withdrawn, both when the electron temperature is closest to the natural state and closest to the saturation state. At these moments, $\partial\sigma/\partial t$ undergoes a sudden change, reaching a peak. Under triangular-wave and sine-wave modulation, since the power versus time curve can be derived, $\partial\sigma/\partial t$ also undergoes continuous variation throughout the modulation process, without any sudden mutation moments, as shown in Figure 3. Under square-wave modulation, the variation amplitudes of $\partial\sigma_H/\partial t$ and $\partial\sigma_P/\partial t$ are much greater than under triangular-wave or sine-wave modulation, resulting in a stronger signal. However, due to frequent sudden changes of $\partial\sigma/\partial t$, the temporal variation curve deviates significantly from the sine waveform, leading to severe distortion in the generated signal. In the process of triangular-wave and sine-wave modulation, the variations in $\partial\sigma/\partial t$ are continuous and the trends of increasing and decreasing heating-wave power are symmetric. The heating and cooling times of electrons are almost equal, which, under the condition of declining amplitude size, also makes the temporal variation curve of $\partial\sigma/\partial t$ more closely approximate the sine waveform, effectively suppressing the generation of harmonics.

3.2 Conductivity Oscillations under Optimized Waveform Modulation

In order to suppress harmonic generation as much as possible and improve the excitation efficiency of the fundamental frequency signal, we modified the three basic waveforms mentioned earlier. Firstly, for the square-wave, we changed its duty cycle. The amplitudes of $\partial\sigma/\partial t$ at different frequencies induced by the modulation of square-waves with 30%, 40% and 60% duty cycles in the ionosphere are shown in Figure 4. From the displayed results, it can be observed that whether the duty cycle is increased or decreased from 50%, the asymmetry of the modulated waveform results in a significant difference in the heating and cooling times of electrons, and the temporal variation trends of $\partial\sigma/\partial t$ deviate more than with a sine function. The even harmonic produced by modulation heating is significantly enhanced relative to a duty cycle of 50%. Reducing the duty cycle below 50% increases the heating wave power injected into the ionosphere during the heating moment, and the peak of $\partial\sigma/\partial t$ is also larger. When the duty cycle is reduced to 30%, the intensity of the second harmonic is comparable to the fundamental frequency signal. As the duty cycle decreases, the intensity of the fundamental frequency signal generated by modulation also increases, but the problem of signal distortion becomes more significant.

For the triangular waveform, we made changes to its slope. The modulation waveform is formulated according to:

$$\begin{cases} \dfrac{1+k}{2}\left(\dfrac{2t}{T}\right)^k P_E & 0 \le t < \dfrac{T}{2}, \\ \dfrac{1+k}{2}\left(2-\dfrac{2t}{T}\right)^k P_E & \dfrac{T}{2} \le t < T, \end{cases} \tag{13}$$

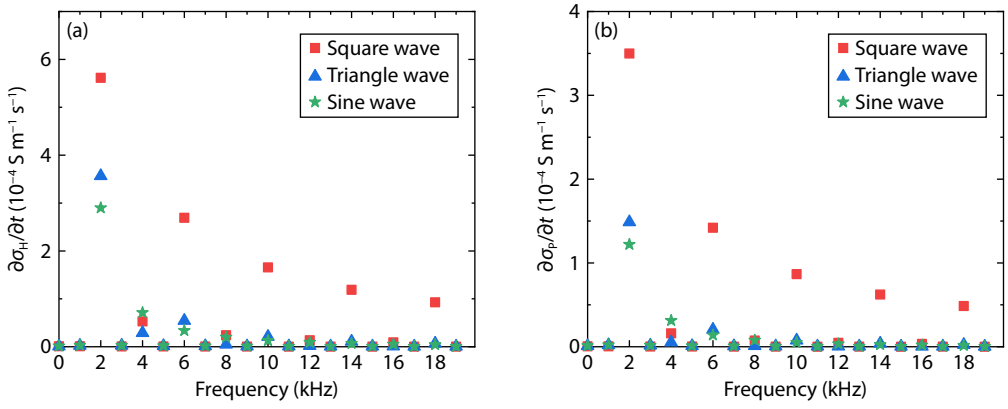

Figure 2. Amplitude of oscillations in the rate of change of conductivity with time at different frequencies, produced by modulation of a square-wave with 50% duty cycle, a triangular-wave, and a sine-wave in the source region of the main ionospheric radiation. Plots (a) and (b) correspond respectively to the Hall conductivity 70 km above ground level and the Pedersen conductivity 73 km above ground level.

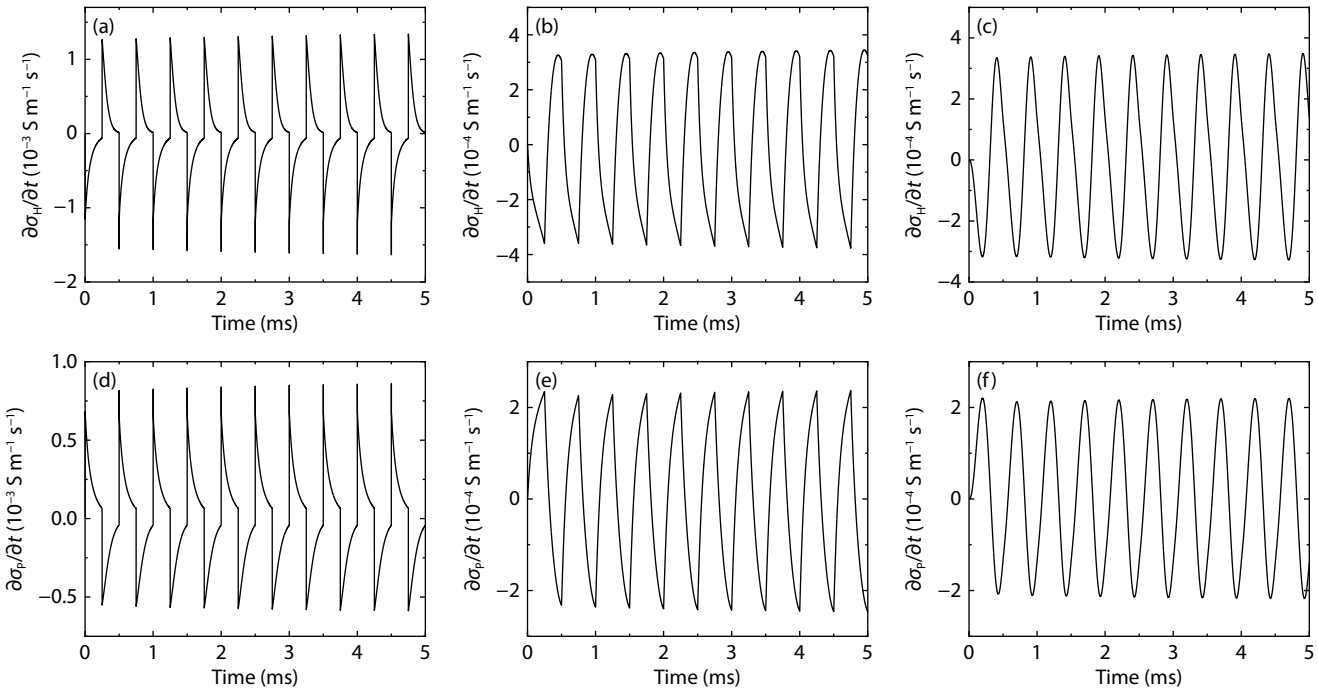

Figure 3. Oscillations in the rate of change of conductivity with time in the main radiation source region of the ionosphere during modulated heating. (a), (b) and (c): Results of changes in Hall conductivity 70 km above ground level for a square-wave with 50% duty cycle, triangular-wave, and sine-wave modulation, respectively. (d), (e) and (f): Results of changes in Pedersen conductivity 73 km above ground level for a square-wave with 50% duty cycle, triangular-wave, and sine-wave modulation, respectively.

where T is the modulation period, P_E is the effective radiation power, and k can be used to adjust to the waveform.

We selected waveforms with k equal to 0.8, 1.2, and 1.5 for simulation calculation, and the modulation result of the three waveforms is shown in Figure 5. It can be seen that when k = 0.8 or 1.2, the ratio of the amplitudes of various harmonics to the intensity of the fundamental frequency signal and the longitudinal size of the radiation source are almost the same as when k = 1 (triangular wave). With an increase of k, the excited fundamental frequency signal also becomes stronger. When k is increased to 1.5, the intensity of even harmonics is significantly enhanced, and the excited ELF/VLF signal no longer follows the characteristic of odd harmonics being stronger than even harmonics, but is closer to the modulation results of the sine wave. The proportion of harmonic energy in the excited signal slightly increases, which does not meet our requirement for minimizing harmonics.

For the sine waveform, we introduced a power exponent k to its waveform function. Since it is difficult to solve the integration of the $\sin^k t$ function, we only focus on the harmonic suppression effect of this waveform, without evaluating the excitation intensity of the signal it generates. The distortion of signals generated by sine-wave modulation for different k values is shown in Figure 6. From the results, it can be seen that with an increase of k, the ELF/VLF signals generated by $\sin^k t$ modulation and the radiation source area still maintain the characteristics of sine-wave modulation. In other words, the intensity of harmonics and the size of the radiation source decrease with increasing frequency. The size of the fundamental wave radiation source remains basically unchanged, while the radiation source area of harmonics significantly shrinks, and the intensity of higher frequency harmonics decreases significantly. When k is increased to 1.5, only the second and third harmonics can be observed in the graph. The proportion of harmonics to the fundamental frequency signal strength continues to decrease, reaching a minimum value around k = 2, indicating the strongest ability to suppress harmonics. Under this waveform modulation, besides the fundamental frequency signal, only a weak amplitude can be observed at the frequency of the second harmonic, while the energy at other harmonic frequencies approaches zero.

We selected sine waveform modulation for different k values, and compared the amplitudes of $\partial\sigma/\partial t$ at various frequencies in the main radiation source area, which is at a height of 70 km above the ground for $\partial\sigma_H/\partial t$, and a height of 73 km for $\partial\sigma_P/\partial t$. Since improving the excitation efficiency of the fundamental frequency signal is not our primary goal, and in order to better observe the proportion of harmonic energy in the signal, we normalized the calculated $\partial\sigma_H/\partial t$ and $\partial\sigma_P/\partial t$. The results are shown in Figure 7. It can be seen that when k increases to 1.8, the amplitude of the second harmonic of $\partial\sigma_H/\partial t$ reaches a minimum value. As k continues to increase, the harmonics of $\partial\sigma_P/\partial t$ become stronger, while the harmonic intensity of $\partial\sigma_H/\partial t$ decreases monotonically. Since $\partial\sigma_H/\partial t$ has a larger oscillating current magnitude than does $\partial\sigma_P/\partial t$, when $k > 1.8$, further increasing k does not significantly enhance the harmonic suppression effect of $\partial\sigma_H/\partial t$, but it will increase the harmonics of $\partial\sigma_P/\partial t$. Therefore, it can be roughly determined that when $k \approx 2$, the harmonics in the signal generated by modulation heating are weakest.

As a last step, we normalize the heating results of square-wave

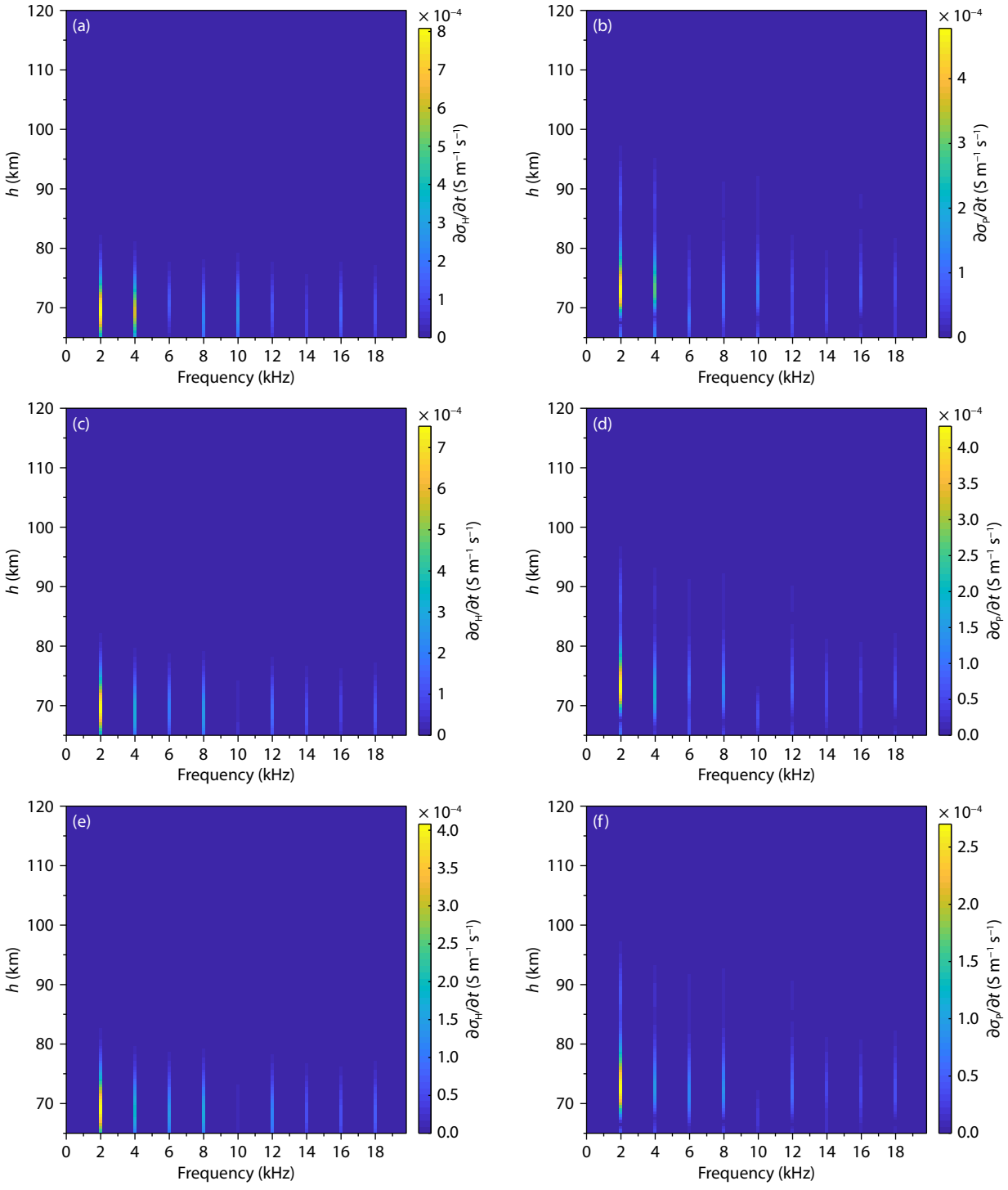

Figure 4. Oscillation amplitudes of the time-dependent rate of change of conductivity in each height region of the ionosphere, induced by square-wave modulated heating with different duty cycles at different frequencies. (a), (c) and (e): Oscillations of Hall conductivity induced by square-wave modulation with 30%, 40%, and 60% duty cycle, respectively. (b), (d) and (f): Oscillations of Pedersen conductivity induced by square-wave modulation with 30%, 40%, and 60% duty cycle, respectively.

with a duty cycle of 50%, triangular-wave, and sine-wave modulation, then compare the degree of signal distortion. Comparisons of $\partial\sigma/\partial t$ results produced by the three modulation waveforms in the main radiation source zone are illustrated in Figure 8. It can be observed from Figure 8 that the ratio of the intensity of the second harmonic to the fundamental frequency signal is almost the same for the three heating waveforms. The amplitude at the second harmonic frequency is less than one-tenth that at the fundamental frequency. However, a characteristic of signals produced by square-wave and triangular-wave modulation is that the intensity of odd harmonics is much greater than that of even harmonics. It can be seen from the figure that significant ampli-

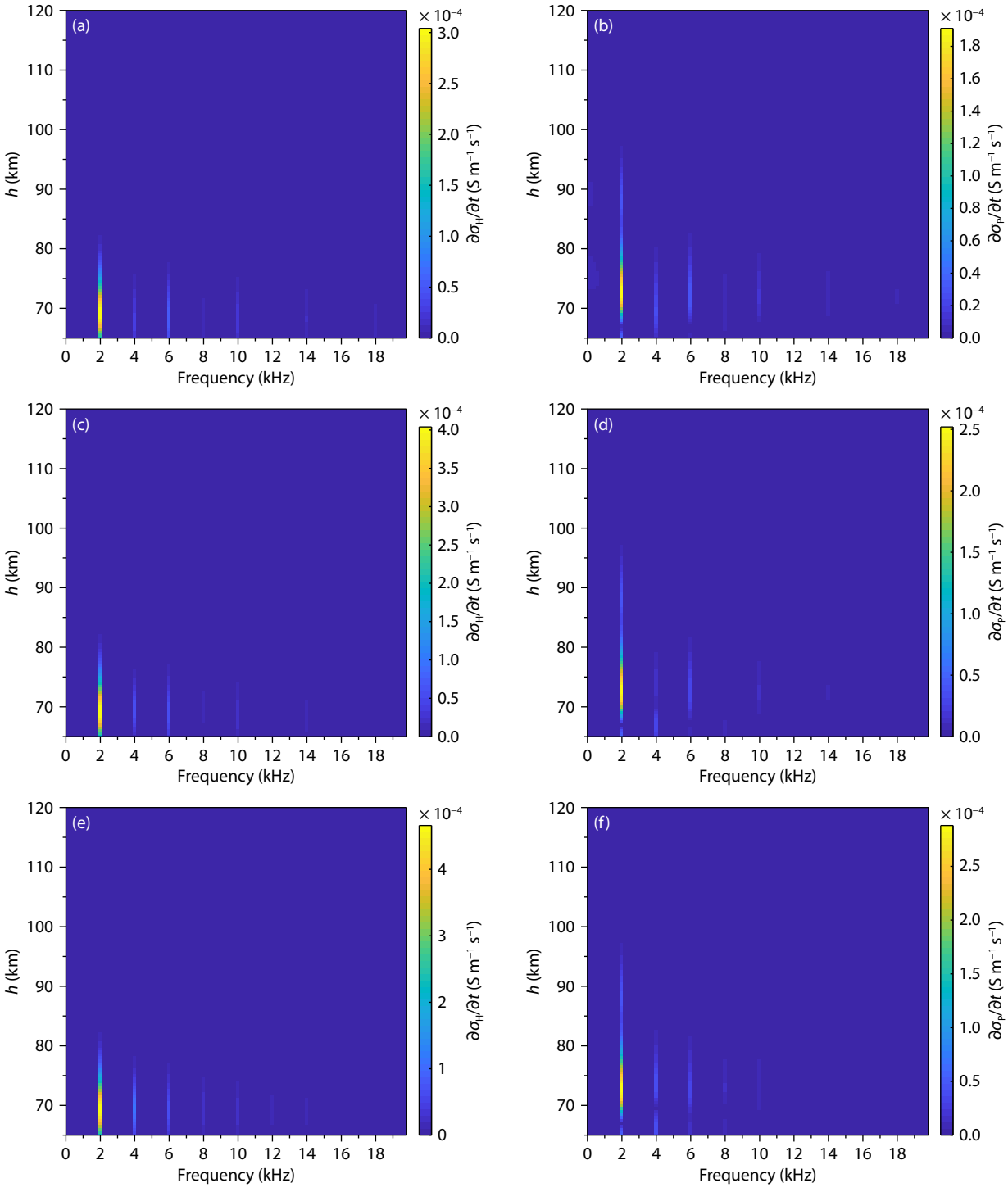

Figure 5. Amplitudes of oscillations in the rate of change of conductivity with time in each height region of the ionosphere, induced by triangular wave modulation heating at different frequencies for different k values. (a), (c), and (e): Oscillation results of Hall conductivity induced by triangular-wave modulation with k = 0.8, 1.2, and 1.5, respectively. (b), (d), and (f): Oscillation results of Pedersen conductivity induced by triangular-wave modulation with k = 0.8, 1.2, and 1.5, respectively.

tudes of $\partial\sigma/\partial t$ exist at 6 kHz and 10 kHz for square-wave and triangular-wave modulation, while under $\sin^2 t$ waveform modulation, apart from the fundamental frequency, there are only weak amplitudes near the second-harmonic frequency, and the harmonics' intensities at other frequencies relative to the fundamental frequency can be neglected.

3.3 Stability of Modulation Waveform Suppression Capability for Harmonics

It is worth noting that the energy relationship between harmonics and the fundamental frequency signal generated under these modulation waveforms remains relatively constant, not changing significantly with variations in heating conditions, thus ensuring a

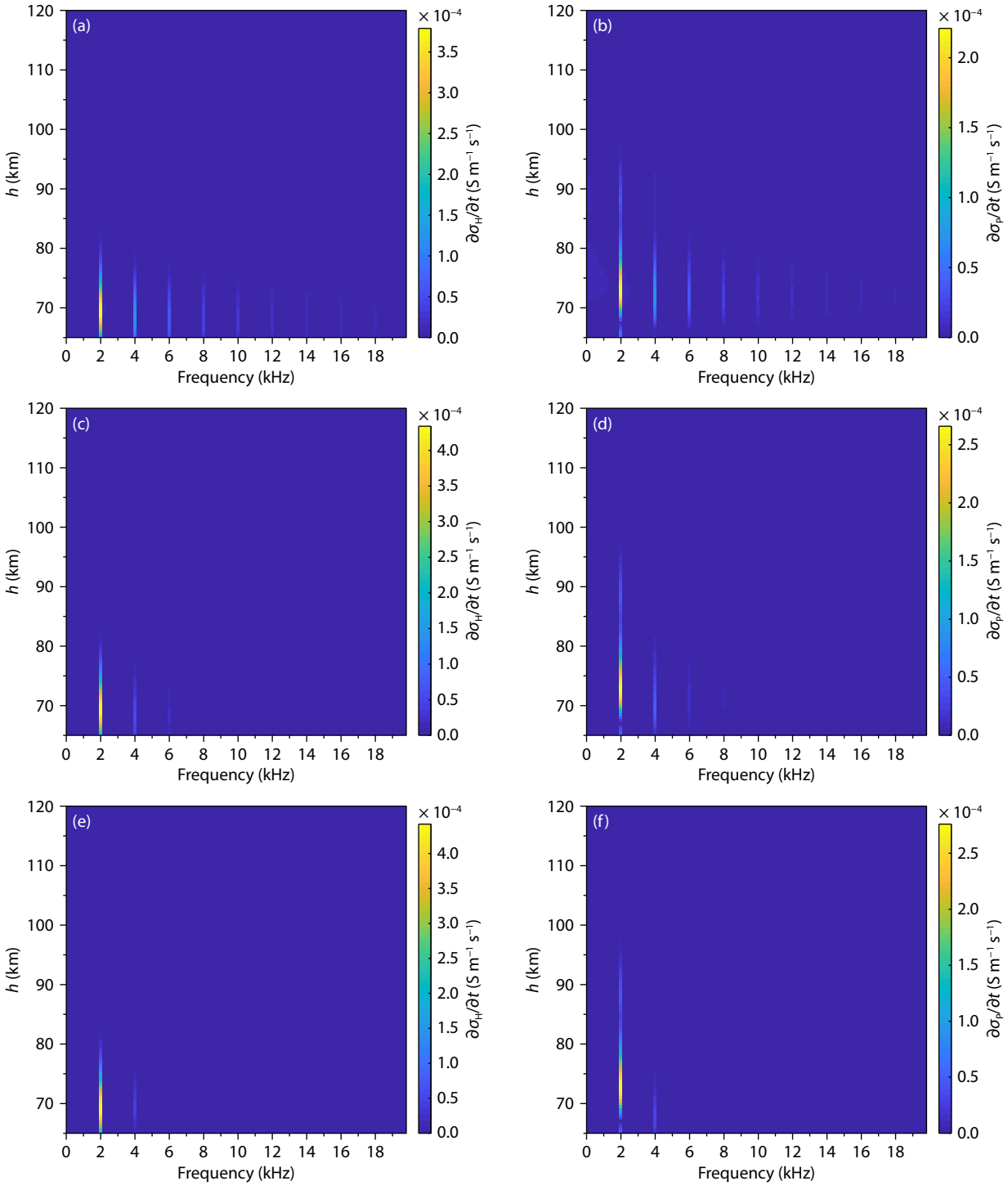

Figure 6. Amplitudes of oscillations in the rate of change of conductivity with time in each height region of the ionosphere, induced by sine-wave modulation heating at different frequencies under different k values. (a), (c), and (e): Oscillation results of Hall conductivity induced by sine wave modulation with k = 0.8, 1.5, and 2.0, respectively. (b), (d), and (f): Oscillation results of Pedersen conductivity induced by sine-wave modulation with k = 0.8, 1.5, and 2.0, respectively.

stable harmonic suppression effect. Taking square-wave modulation heating with a duty cycle of 50% as an example, we vary the effective radiation power and modulation frequency to observe whether the modulation waveform's ability to suppress harmonics changes for different heating conditions. Figure 9 presents the heating results of square-wave modulation with modulation frequencies of 2000 Hz and effective radiation powers of 32 MW and 48 MW, respectively, and with a modulation frequency of 4000 Hz and an effective radiation power of 16 MW. The results indicate that with an increase in effective radiation power, both the fundamental frequency signal and harmonic intensity generated by modulation increase. However, regardless of changes in

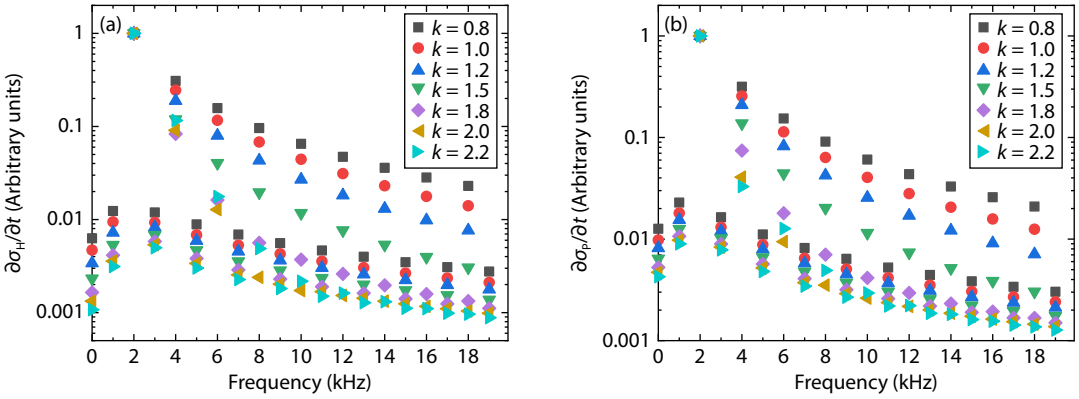

Figure 7. Ratio of harmonic signal intensity at different frequencies produced by sine wave modulation at different values of k to the fundamental frequency signal intensity in the main radiation source region of the ionosphere. (a) and (b) correspond respectively to Hall conductivity at 70 km above ground level and Pedersen conductivity at 73 km above ground level.

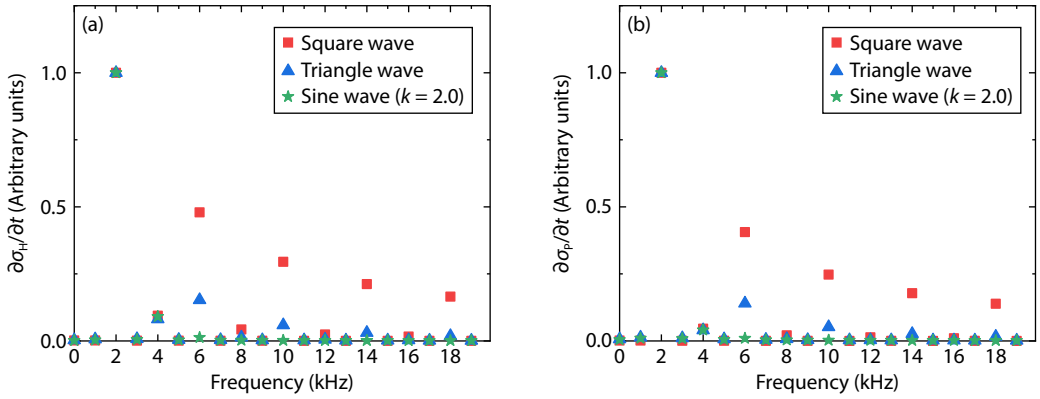

Figure 8. Ratios of harmonic signal intensity at different frequencies to fundamental frequency signal intensity generated by modulation of a square-wave with 50% duty cycle, a triangular-wave, and a sine wave (k = 2.0) in the main radiation source region of the ionosphere. (a) For Hall conductivity at 70 km above ground level. (b) For Pedersen conductivity at 73 km above ground level.

modulation frequency or effective radiation power, the modulation waveform's ability to suppress harmonics remains unchanged, maintaining the characteristic of odd harmonics' energy being greater than that of even harmonics. Only the overall intensity of the excited signal changes, and the position of the main radiation source zone shifts slightly upwards with the increase in effective radiation power. The duration of one cycle of modulation heating is on the millisecond scale, and the change in electron density during this time scale is not significant. The change in conductivity comes mainly from the oscillation of electron temperature. The increase in effective radiation power increases the amplitude of electron temperature oscillation, thereby enhancing the signal intensity. Increasing the modulation frequency shortens the period, making abrupt changes of $\partial\sigma/\partial t$ in modulation heating more frequent, thereby increasing the excitation efficiency of ELF/VLF signals to some extent.

4. Conclusion

In this study, a simulation model of amplitude-modulation heating is established, using a square wave with a duty cycle of 50%, a triangular-wave, and a sine-wave as the basic modulation waveforms for simulation. Other waveforms are considered for testing, based on these basic waveforms, and the results are compared and analyzed. The results indicate that among these three basic waveforms, the signals generated by a square-wave with a duty cycle of 50% and triangular-wave modulation both exhibit the characteristic of more intense odd harmonics than even harmonics. Among the waveforms, the signal excited by square-wave modulation is the strongest, while the signal excited by triangular-wave modulation has the smallest proportion of harmonic energy. The modulation results of the sine-wave do not exhibit any obviously different characteristics than the first two, with triangular-wave modulation being the weakest fundamental frequency signal excited and the least able to suppress harmonics. After modifying these basic waveforms, it was found that reducing the duty cycle is more conducive to increasing the intensity of the fundamental frequency signal generated by square-wave modulation, but the proportion of harmonic energy in the signal also increases, resulting in greater signal distortion. Changing the slope of the triangular-wave does not yield the desired results, and the modified waveform's ability to suppress harmonics is even weaker than that of the basic triangular waveform. Through testing, we determined that the harmonic radiation source size generated by a $\sin^2 t$ modulation waveform is the smallest, and the harmonic signal is the weakest. At the main radiation source zone, the amplitude of the second harmonic is less than one-tenth that

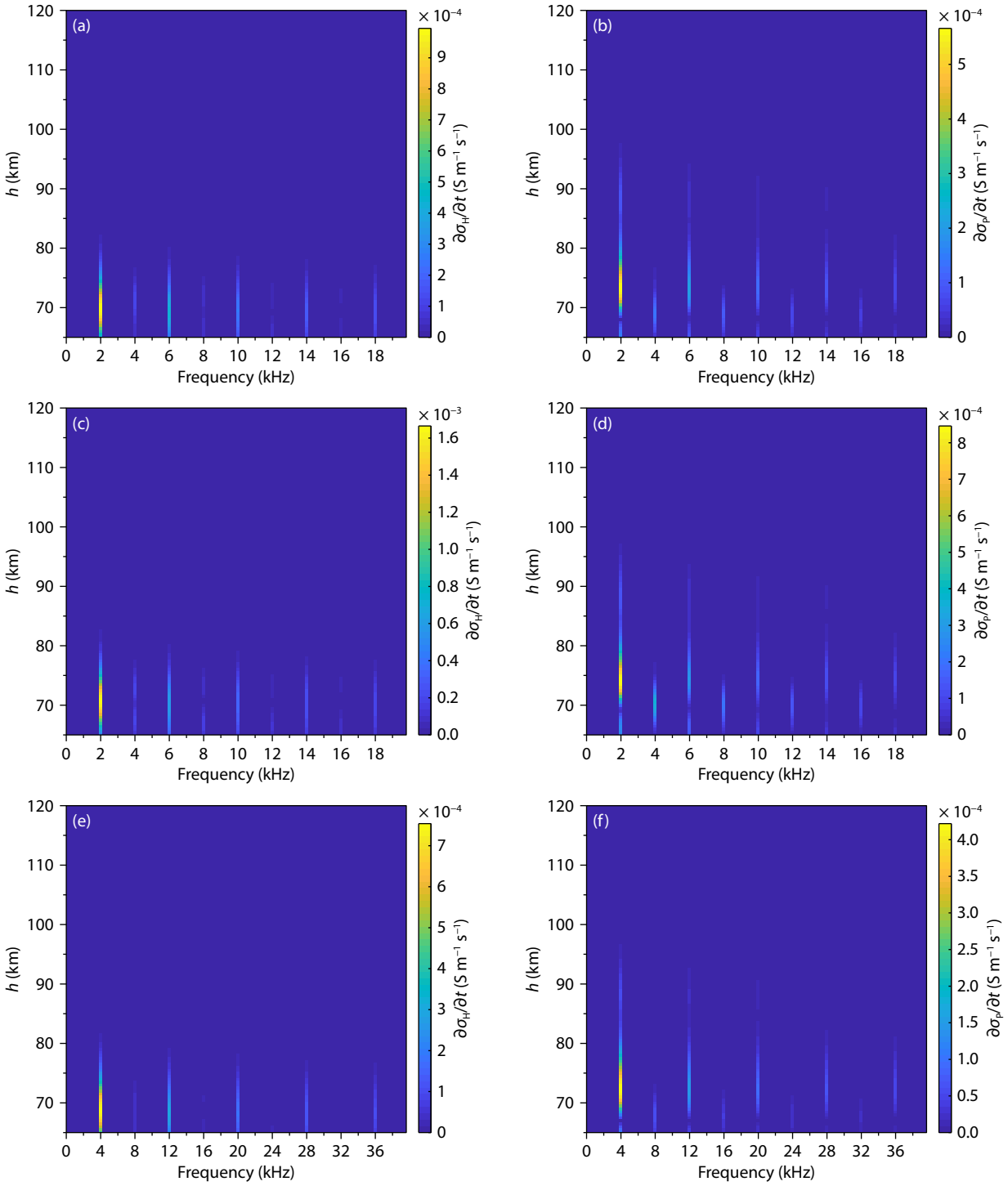

Figure 9. The oscillation amplitudes of the temporal variation rates of conductivity within various altitude regions of the ionosphere induced by square-wave modulation heating with a 50% duty cycle at different effective radiation powers and modulation frequencies. (a), (c), and (e): Oscillation outcomes of the Hall conductivity induced by square-wave modulation heating with modulation frequencies of 2000 Hz and effective radiation powers of 32 MW and 48 MW, and with a modulation frequency of 4000 Hz and an effective radiation power of 16 MW, respectively. (b), (d), and (f): Correspondingly oscillation outcomes of the Pedersen conductivity induced by square-wave modulation heating with modulation frequencies of 2000 Hz and effective radiation powers of 32 MW and 48 MW, and with a modulation frequency of 4000 Hz and an effective radiation power of 16 MW, respectively.

of the fundamental wave, and the energy proportion of harmonics in other frequency bands is too small to be considered.

In addition, when taking square-wave modulation with a duty cycle of 50% as an example, it was found that the proportion of harmonic energy in the signal excited by a fixed modulation waveform is unaffected by changes of the effective radiated power and modulation frequency. Only the overall signal intensity

changes, indicating that the modulation waveform's ability to suppress harmonics remains stable during changes in heating conditions. From the simulation results, it can be observed that increasing the effective radiation power effectively enhances the signal intensity, with the position of the main radiation source zone shifting slightly upwards.

In summary, during modulation heating, using square-wave modulation with a small duty cycle can effectively enhance the excitation efficiency of the signal, while using a $\sin^2 t$ waveform modulation can effectively suppress harmonic generation and prevent signal distortion. It is difficult to determine a modulation waveform that simultaneously meets the requirements of both efficient signal excitation and harmonic suppression. However, we can first use a $\sin^2 t$ waveform to ensure that the proportion of harmonic energy is as small as possible, then increase the effective radiation power until the signal is enhanced to meet requirements for communication applications .

Acknowledgments

This work was supported by the National Key R&D Program of China (No. 2022YFE0204100), the National Natural Science Foundation of China (12205067 and 12375199), and the Fundamental Research Funds for the Central Universities (Grant No. HIT.OCEF. 2022036).

Data Availability

The data that support the findings of this study are available from their corresponding authors upon reasonable request.

References

Bailey, V. A., and Martyn, D. F. (1934). The influence of electric waves on the ionosphere. *London, Edinburgh, Dublin Philos. Mag. J. Sci.*, *18*(118), 369–386. https://doi.org/10.1080/14786443409462506

Cohen, M. B., Inan, U. S., and Golkowski, M. A. (2008). Geometric modulation: A more effective method of steerable ELF/VLF wave generation with continuous HF heating of the lower ionosphere. *Geophys. Res. Lett.*, *35*(12), L12101. https://doi.org/10.1029/2008GL034061

Cohen, M. B., Inan, U. S., Gołkowski, M., and Lehtinen, N. G. (2010). On the generation of ELF/VLF waves for long-distance propagation via steerable HF heating of the lower ionosphere. *J. Geophys. Res.: Space Phys.*, *115*(A7), A07322. https://doi.org/10.1029/2009JA015170

Cohen, M. B., and Gołkowski, M. (2013). 100 days of ELF/VLF generation via HF heating with HAARP. *J. Geophys. Res.: Space Phys.*, *118*(10), 6597–6607. https://doi.org/10.1002/jgra.50558

Farley, D. T. Jr. (1963). A plasma instability resulting in field-aligned irregularities in the ionosphere. *J. Geophys. Res.*, *68*(22), 6083–6097. https://doi.org/10.1029/JZ068i022p06083

Ferraro, A. J., Lee, H. S., Allshouse, R., Carroll, K., Tomko, A. A., Kelly, F. J., and Joiner, R. G. (1982). VLF/ELF radiation from the ionospheric dynamo current system modulated by powerful HF signals. *J. Atmos. Terr. Phys.*, *44*(12), 1113–1122. https://doi.org/10.1016/0021-9169(82)90022-8

Ferraro, A. J., Lee, H. S., Allshouse, R., Carroll, K., Lunnen, R., and Collins, T. (1984). Characteristics of ionospheric ELF radiation generated by HF heating. *J. Atmos. Terr. Phys.*, *46*(10), 855–865. https://doi.org/10.1016/0021-9169(84)90025-4

Getmantsev, G. G., Zuikov, N. A., Kotik, D. S., Mironenko, L. F., Mityakov, N. A., Rapoport, V. O., Sazonov, Y. A., Trakhtengerts, V. Y., and Éidman, V. Y. (1974). Combination frequencies in the interaction between high-power short-wave radiation and ionospheric plasma. *JETP Lett.*, *20*(4), 101–102.

Gurevich, A. V. (1976). Nonlinear phenomena in the ionosphere. *Radiophys. Quantum Electron.*, *19*(6), 595–597. https://doi.org/10.1007/BF01043546

Jin, G., Spasojevic, M., Cohen, M. B., and Inan, U. S. (2012). Harmonic minimization waveforms for modulated heating experiments at HAARP. *J. Geophys. Res.: Space Phys.*, *117*(A11), A11315. https://doi.org/10.1029/2012JA018102

Kuo, S. P., Faith, J., Lee, M. C., and Kossey, P. (1998). Numerical comparison of two schemes for the generation of ELF and VLF waves in the HF heater-modulated polar electrojet. *J. Geophys. Res.: Space Phys.*, *103*(A3), 4063–4069. https://doi.org/10.1029/97JA02535

Kuo, S. P. (2018). *Plasma Physics in Active Wave Ionosphere Interaction*. New York: New York University-Tandon School of Engineering.

Li, H., and Wu, J. (2021). Dielectric permittivity of dusty plasma in the Earth's mesosphere. *Earth Planet. Phys.*, *5*(1), 117–120. https://doi.org/10.26464/epp2021006

Li, J. F., Wang, Y., Zhou, Z. X., Yao, J. F., Liu, J. L., Lan, Z. H., and Yuan, C. X. (2023a). Experimental observations of communication in blackout, topological waveguiding and Dirac zero-index property in plasma sheath. *Nanophotonics*, *12*(10), 1847–1856. https://doi.org/10.1515/nanoph-2022-0800

Li, J. F., Yao, J. F., Wang, Y., Zhou, Z. X., Kudryavtsev, A. A., Lan, Z. H., and Yuan, C. X. (2023b). Observation of nontrivial Zak phase induced topological states in glow discharge plasma. *APL Photon.*, *8*(6), 066102. https://doi.org/10.1063/5.0149985

Li, Y., Li, H., Wu, J., Lyu, X. B., Yuan, C. X., Li, C., and Zhou, Z. X. (2023c). Effect of wave polarization on ionospheric Ohmic heating and optimal polarization. *Phys. Plasmas*, *30*(10), 102902. https://doi.org/10.1063/5.0158960

Lu, H., Yang, J. T., Li, Q. L., Hao, S. J., Guo, F., Wu, J., Chen, J., Ma, G. L., and Xu, T. (2021). ELF/VLF communication experiment by modulated heating of ionospheric auroral electrojet at EISCAT. *IEEE Trans. Antennas Propagat.*, *69*(4), 2267–2273. https://doi.org/10.1109/TAP.2020.3026872

Milikh, G. M., and Papadopoulos, K. (2007). Enhanced ionospheric ELF/VLF generation efficiency by multiple timescale modulated heating. *Geophys. Res. Lett.*, *34*(20), L20804. https://doi.org/10.1029/2007GL031518

Moore, R. C., Inan, U. S., Bell, T. F., and Kennedy, E. J. (2007). ELF waves generated by modulated HF heating of the auroral electrojet and observed at a ground distance of ~4400 km. *J. Geophys. Res.: Space Phys.*, *112*(A5), A05309. https://doi.org/10.1029/2006JA012063

Papadopoulos, K., Chang, C. L., Vitello, P., and Drobot, A. (1990). On the efficiency of ionospheric ELF generation. *Radio Sci.*, *25*(6), 1311–1320. https://doi.org/10.1029/RS025i006p01311

Pashin, A. B., Belova, E. G., and Lyatsky, W. B. (1995). Magnetic pulsation generation by a powerful ground-based modulated HF radio transmitter. *J. Atmos. Terr. Phys.*, *57*(3), 245–252. https://doi.org/10.1016/0021-9169(93)E0005-T

Rietveld, M. T., Kopka, H., and Stubbe, P. (1986). *D*-region characteristics deduced from pulsed ionospheric heating under auroral electrojet conditions. *J. Atmos. Terr. Phys.*, *48*(4), 311–326. https://doi.org/10.1016/0021-9169(86)90001-2

Rowland, H. L., Keskinen, M. J., Villaseñor, J. S., and Wong, A. Y. (1996). Observations and simulations of VLF harmonic generation with the high-power auroral simulation array. *J. Geophys. Res.: Space Phys.*, *101*(A12), 27027–27033. https://doi.org/10.1029/96JA02331

Streltsov, A. V., Berthelier, J. J., Chernyshov, A. A., Frolov, V. L., Honary, F., Kosch, M. J., McCoy, R. P., Mishin, E. V., and Rietveld, M. T. (2018). Past, present and future of active radio frequency experiments in space. *Space Sci. Rev.*, *214*(8), 118. https://doi.org/10.1007/s11214-018-0549-7

Stubbe, P., and Varnum, W. S. (1972). Electron energy transfer rates in the ionosphere. *Planet Space Sci.*, *20*(8), 1121–1126. https://doi.org/10.1016/0032-0633(72)90001-3

Tellegen, B. D. H. (1933). Interaction between Radio-waves?. *Nature, 131*(3319), 840. https://doi.org/10.1038/131840a0

Utlaut, W. F. (1970). An ionospheric modification experiment using very high power, high frequency transmission. *J. Geophys. Res.*, *75*(31), 6402–6405. https://doi.org/10.1029/JA075i031p06402

Utlaut, W. F., and Violette, E. J. (1974). A summary of vertical incidence radio observations of ionospheric modification. *Radio Sci.*, *9*(11), 895–903. https://doi.org/10.1029/RS009i011p00895

Willis, J. W., and Davis, J. R. (1973). Radio frequency heating effects on electron density in the lower *E* region. *J. Geophys. Res.*, *78*(25), 5710–5717. https://doi.org/10.1029/JA078i025p05710

Yang, J. T., Wang, J. G., Li, Q. L., Wu, J., Che, H. Q., Ma, G. L., and Hao, S. J. (2019). Experimental comparisons between AM and BW modulation heating excitation of ELF/VLF waves at EISCAT. *Phys. Plasmas*, *26*(8), 082901. https://doi.org/10.1063/1.5095537

Zhou, K. J., Wang, H. L., and Cao, P. P. (2020). Theoretical analysis of parameter optimization for lower-ionosphere excitation ELF/VLF waves based on chirp-BOK modulated heating. *IEEE Access*, *8*, 165646–165657. https://doi.org/10.1109/ACCESS.2020.3022171